Modeling Radiation Damage to Pixel Sensors in the ATLAS Detector

Tomáš Dado, On behalf of the ATLAS collaboration[a,*]

[a]*TU Dortmund*
Otto-Hahn-Str. 4a, 44227 Dortmund, Germany

E-mail: tomas.dado@cern.ch

Silicon pixel detectors are at the core of the current and planned upgrade of the ATLAS detector at the Large Hadron Collider (LHC). As the closest detector component to the interaction point, these detectors will be subjected to a significant amount of radiation over their lifetime: prior to the High-Luminosity LHC (HL-LHC), the innermost layers will receive a fluence of $1 - 5 \times 10^{15}$ 1 MeV n_{eq}/cm^2 and the HL-LHC detector upgrades must cope with an order of magnitude higher fluence integrated over their lifetimes. Simulating radiation damage is critical in order to make accurate predictions for current future detector performance. A model of pixel digitization is presented that includes radiation damage effects to the ATLAS pixel sensors for the first time. In addition to a thorough description of the setup, predictions are presented for basic pixel cluster properties alongside early studies with LHC Run 2 proton-proton collision data.

---

[*]Speaker

1. Introduction

The Inner Detector (ID) of the ATLAS detector [1] is the component closest to the interaction point. The purposes of the sub-detector are pattern recognition of tracks, momentum measurement of the charged particles, vertex identification and electron identification. The ID consists of three sub-detectors: Pixel Detector, Semiconductor Tracker (SCT) and Transition-Radiation Tracker (TRT). The Pixel detector [2] is closest to the interaction point, thus it suffers the most from the radiation damage. The Pixel detector consists of four layers, with the innermost layer being Insertable B Layer (IBL) [3] that was installed between the Run 1 and Run 2 of Large Hadron Collider (LHC), and three disk layers on each side of the barrel. The sensors in the barrel and disk layers are composed of n^+-in-n planar oxygenated silicon sensors at radii of 33.25 mm, 50.5 mm, 88.5 mm and 122.5 mm, from the centre of the ATLAS detector. The IBL sensors are 200 μm thick, while the sensors in other layers are 250 μm thick. The forward regions of the innermost layer contain n^+-in-p 3D sensors that are 230 μm thick.

Radiation damage in the sensor bulk causes displacement of the silicon atom out of its lattice, resulting in a silicon interstitial site and a leftover vacancy. These defects lead to microscopic effects: a change in the effective doping concentration, trapping of the charges and increase in the sensor leakage currents. The microscopic effects result in several macroscopic effects. A change in the doping concentration leads to a change in the depletion voltage as well as electric field profiles that impact the mobility of the charges. The trapping of the charges results in a reduced signal collection efficiency. Annealing effects further complicate the estimation of the irradiation effects as the radiation damage effects depend both on the irradiation as well as the temperature history.

2. Fluence estimation

The radiation fields from the collisions are estimated by propagating inelastic proton–proton interactions, simulated by Pythia 8 [4, 5], through the ATLAS detector material using the FLUKA code [6, 7] for the particle transport simulation. Prediction of the 1 MeV n_{eq} per fb^{-1} for the central part of the IBL is $6.2 \times 10^{12}\, n_{eq}/\text{cm}^2/\text{fb}^{-1}$. Using the total Run 2 luminosity of about 160 fb^{-1} measured with dedicated sub-detectors, the total fluence for the central part of the IBL reaches $10^{15} n_{eq}/\text{cm}^2$.

Exploiting the fact that the amount of received fluence changes the sensor leakage current, by measuring the leakage current the fluence can be measured. Using the Hamburg model [8] for the predicted leakage current as a function of the fluence for all Pixel layers, the predicted and the measured leakage currents as well as the fluence are estimated [9]. Figure 1 shows the comparison for the total fluence received during Run 2 for the Pixel layers as well as the disks. A good agreement between the simulation and the measurement is seen in the central parts of the IBL, however, the leakage current measurement shows much stronger dependence on z than the prediction. Furthermore, the magnitude of the fluence in the other layers is underestimated in the prediction. The discrepancy between the prediction and the measurement originates from multiple sources: imprecise measurement of the temperature history, definition of the depletion voltage and its measurement, as well as modelling of the particles and approximations used in the radiation damage models.
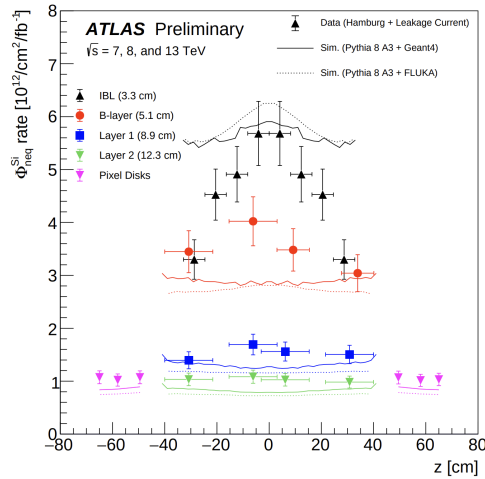
Figure 1: The fluence-to-luminosity conversion factors as a function of z, compared with the Pythia 8 (A3 tune) +FLUKA and Pythia 8 (A3 tune)+Geant4 predictions [9].

3. ATLAS digitizer scheme

The effects of the radiation damage to the silicon sensor can be enabled in the ATLAS digitization step, i.e. the step in the ATLAS Monte Carlo simulation where the energy deposits from the charged particles are converted to the digital signals of the read-out system. The simulation aims to reflect the microscopic changes in the silicon bulk due to the radiation damage using an effective model to reduce the processing time. The digitization algorithm [10] is as follows. Firstly, the position and the magnitude of the energy deposits are received from the GEANT4 simulation. The ionisation energy is then converted into electron-hole pairs that are then grouped to speed up the simulation. For each charge group, a fluence-dependent time-to-trap is randomly generated and compared with the drift time due to electric and magnetic fields. If the drift time is larger than the trapping time, the charge group is declared trapped. Since moving charges induce a current in the collecting electrode, a signal is induced on the electrodes also from trapped charges while they still drift. The induced charge is calculated using the weighting (Ramo) potential with the known trapped position. The total induced charge is then converted to the time-over-threshold that is used further in the track reconstructions. The induced charge is not only considered for the incident pixel, but also for the neighbouring ones.

To properly propagate the impact of the radiation damage, the electric field in the pixel cells need to be estimated. The electric fields are simulated using the default two-trap Technology Computer Aided Design (TCAD) model. Irradiation effects are simulated using the Chiochia model [11]. Figure 2 shows the z-component (z-axis goes from the electronics chip to the backplane of the sensor) of the electric field as a function of the bulk depth for various irradiation levels. The figure shows that for irradiated sensors, the electric field is no longer linear and it reaches a minimum around the centre of the sensor for high fluences. The variations inside the model lead to up to 30%

variations in the electric field strength. The impact of the annealing has been studied and was found to be minor (3%) on the acceptor trap concentration so the effect is neglected. For more details, see Ref. [10].
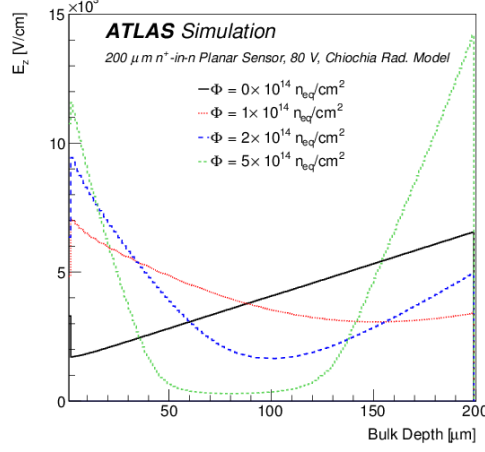
Figure 2: The simulated electric field magnitude in the z direction along the bulk depth, averaged over x and y for an ATLAS IBL sensor biased at 80 V for various fluences [10].

The simulation of the charge drifting can be computationally very expensive, however, it can be pre-computed once per geometry and a set of conditions (bias voltage, temperature and fluence). The electrons and holes drift with a velocity $\vec{v}(E) \sim r\mu(E)\vec{E}$, where r is the Hall scattering factor set to 1 and μ is the mobility. The charge collection time is estimated via

$$t_{\text{collection}}\left(\vec{x}_{\text{initial}}\right) = \int_C \frac{ds}{\mu(E)E},$$ (1)

where C is the path from the initial position, $\vec{x}_{\text{initial}}$, to the final position. The integral in Eq. 1, simplifies to a one-dimensional integral for a planar sensor. For the trapped charges, the position of the trapping can be calculated using $\vec{x}_{\text{trap}}\left(t_{\text{to trap}}\right) = \int_0^{t_{\text{to trap}}} \mu(E)\vec{E}\,dt$, using the known trapping time from Eq. 1.

In the simulation, the trapping time is set randomly from an exponential distribution with mean value $1/(\beta\Theta)$, where β is the trapping constant and Θ is the fluence. For the simulation, the trapping constants are set to $\beta_e = (4.5 \pm 1.5) \times 10^{-16}$ cm^2/ns for electrons, and $\beta_h = (6.5 \pm 1.5) \times 10^{-16}$ cm^2/ns for holes.

The Lorentz angle (θ_{L}) is the result of balancing electric and magnetic forces, and is defined as the incidence angle that produces the smallest cluster size in the transverse direction. Due to the changes in the electric field due to irradiation, and having the same magnetic field, the Lorentz angle changes with increased fluences. The tangent of the Lorentz angle, $\tan\theta_{\text{L}}^{\text{integrated}}$, can be calculated as

$$\tan\theta_{\text{L}}^{\text{integrated}} = \frac{B}{|z_{\text{final}} - z_{\text{initial}}|} \int_{z_{\text{initial}}}^{z_{\text{final}}} \mu(E(z))\,dz,$$ (2)

where B is the magnetic field strength. Figure 3 shows the tangent of the Lorentz angle as a function of the starting depth (left) and Lorentz angle as a function of delivered luminosity in 2017

4

as measured in data as well as the prediction. It can be seen that the largest Lorentz angle for highly irradiated sensor is seen for charges starting in the central part of the sensor, which coincides with the smallest electric field (see Figure 2). Comparison of the predicted Lorentz angle as a function of the luminosity shows that the simulation can reproduce the Lorentz angle seen in data.
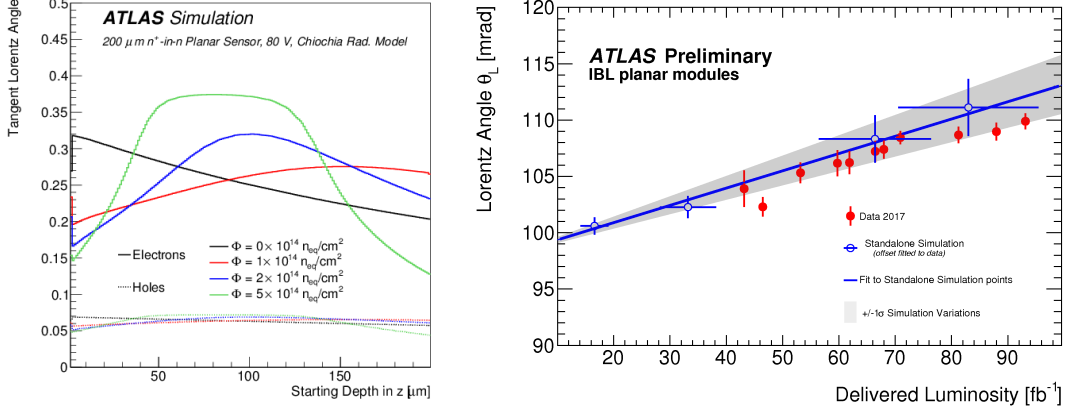

Figure 3: Left: The depth dependence of the Lorentz angle for electrons and holes for four fluences in an ATLAS IBL planar sensor biased at 80 V [10]. Right: Lorentz angle as a function of delivered luminosity in 2017 [12]. Prediction (on blue) and measured data (red) are shown.

The last component of the digitization model is the calculation of the Ramo potential, as the induced charge, Q_{induced} is calculated as

$$Q_{\text{induced}} = -q \left(\phi_W \left(\vec{x}_{\text{end}} \right) - \phi_W \left(\vec{x}_{\text{start}} \right) \right), \tag{3}$$

where q is the electric charge of the charge group and ϕ_W is the Ramo potential. The Ramo potential is pre-calculated by solving the Poisson equation using TCAD. For the planar sensor, the potential varies mainly in the z direction, however, also the x and y components need to be calculated to induce charge on the neighbouring sensors. Figure 4 displays the fraction of the deposited charge collected by a pixel as a function of the bias voltage at the end of 2017 and the end of Run 2 (2018) as predicted by the simulation as well as measured in data. Several interesting observations can be made. Firstly, the figure shows the difficulty in defining the depletion voltage for an irradiated sensor, as the collected charge increases with the bias voltage. The dependency follows approximately a square-root function up to some point and then it turns into a linear dependence. Secondly, it can be seen that the prediction is close to the measurement in terms of the magnitude, but more importantly, the shape of the dependence can also be reproduced in the simulation.

Although most of the pixel sensors in the ATLAS detector are planar sensors, the forward regions of the IBL also use 3D sensors. There are several significant differences in the simulation of the 3D sensors compared to the planar sensors. The effects of the irradiation are simulated using the Perugia model [14] due to the sensors having p-type bulk. The electric field in the 3D sensors is mostly independent of z and charges drift in the x—y plane. The computation of the time to reach the electrodes in Eq. (1) is more complex, since the integral does not simplify to a one dimensional one. Due to the electric field being almost parallel to the magnetic field, the Lorentz angle is negligible in the 3D sensors.
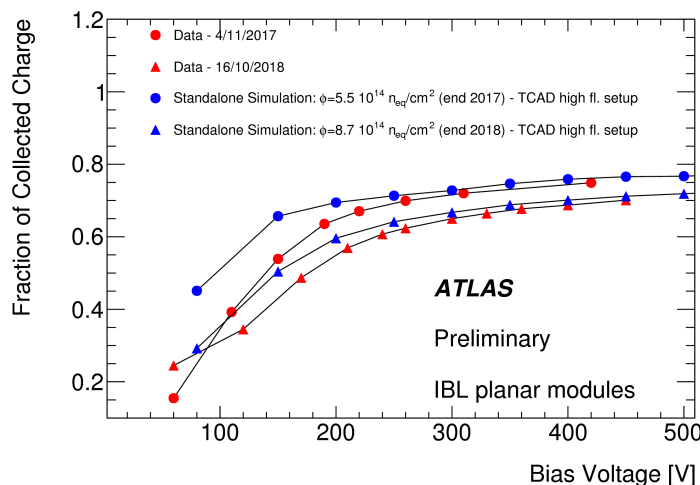
Figure 4: Fraction of the collected charge as a function of the bias voltage for an IBL planar sensor [13]. Both simulation (blue) and data (red) are shown for 2017 (dots) and end of Run 2 (triangles) conditions.

4. Conclusions

These proceedings presented the ATLAS simulation model that incorporates the microscopic effects of the irradiation into a computing efficient model. Significant improvement in radiation-sensitive observables is seen in comparison with data measurements when the effects of the radiation damage are included in the simulation. Run 3 of the LHC as well as High-Lumi LHC (HL-LHC) is expected to deliver significantly more luminosity. In the case of the HL-LHC, an order of magnitude more fluence is expected. With high fluences, several assumptions of the model would need to be revisited: effects of the annealing as well as the dependence of the trapping constants on the fluence.

References

[1] ATLAS Collaboration, *The ATLAS Experiment at the CERN Large Hadron Collider*, *JINST* **3** (2008) S08003.

[2] ATLAS Collaboration, *ATLAS pixel detector electronics and sensors*, *JINST* **3** (2008) P07007.

[3] B. Abbott et al., *Production and Integration of the ATLAS Insertable B-Layer*, *JINST* **13** (2018) T05008 [1803.00844].

[4] T. Sjöstrand, S. Mrenna and P. Skands, *PYTHIA 6.4 physics and manual*, *Journal of High Energy Physics* **05** (2006) 026.

[5] T. Sjöstrand, S. Ask, J. R. Christiansen, R. Corke, N. Desai, P. Ilten et al., *An introduction to pythia 8.2*, *Computer Physics Communications* **191** (2015) 159.

[6] G. Battistoni, F. Cerutti, A. Fassò, A. Ferrari, S. Muraro, J. Ranft et al., *The fluka code: description and benchmarking*, *AIP Conference Proceedings* **896** (2007) 31.

[7] A. Ferrari, P. R. Sala, A. Fassò and J. Ranft, *FLUKA: A multi-particle transport code (program version 2005)*, CERN Yellow Reports: Monographs. CERN, Geneva, 2005, 10.5170/CERN-2005-010.

[8] M. Moll, *Radiation damage in silicon particle detectors: Microscopic defects and macroscopic properties*, Ph.D. thesis, Hamburg U., 1999.

[9] ATLAS Collaboration, *Measurements of sensor radiation damage in the ATLAS inner detector using leakage currents*, *JINST* **16** (2021) P08025 [2106.09287].

[10] ATLAS Collaboration, *Modelling radiation damage to pixel sensors in the ATLAS detector*, *Journal of Instrumentation* **14** (2019) P06012.

[11] V. Chiochia et al., *A Double junction model of irradiated silicon pixel sensors for LHC*, *Nucl. Instrum. Meth. A* **568** (2006) 51 [physics/0506228].

[12] ATLAS Collaboration, "Radiation damage to the atlas pixel and lorentz angle." https://atlas.web.cern.ch/Atlas/GROUPS/PHYSICS/PLOTS/PIX-2017-005/.

[13] ATLAS Collaboration, "Charge collection efficiency as a function of integrated luminosity." https://atlas.web.cern.ch/Atlas/GROUPS/PHYSICS/PLOTS/PIX-2017-004/.

[14] F. Moscatelli, D. Passeri, A. Morozzi, R. Mendicino, G.-F. Dalla Betta and G. M. Bilei, *Combined bulk and surface radiation damage effects at very high fluences in silicon detectors: Measurements and tcad simulations*, *IEEE Transactions on Nuclear Science* **63** (2016) 2716.